Weldline Strength in Injection Molded HDPE/PA6 Blends: Influence of Interfacial Modification

S. FELLAHI, B. FISA,* and B. D. FAVIS

Centre de Recherche Appliquée Sur Les Polymeres (CRASP), Ecole Polytechnique de Montréal, P.O. Box 6079, Station "Centre-ville," Montréal, Québec, Canada H3C 3A7

SYNOPSIS

Most injection molded objects contain defects known as weldlines. This defect may introduce an element of weakness affecting the object's performance. Weldlines are particularly problematic in multiphase materials where the situation may be exaggerated by component mismatch on the two sides of the interface that results in additional weakening when the two components do not adhere well to each other. In addition, weldline behavior is influenced by orientation and morphological effects. This paper deals with relationships between the structure and the mechanical properties in injection molded high density polyethylene polyamide-6 blends. The weldline effect is investigated in detail. Two molds were used to generate weldlines: a double-gated tensile bar cavity in which the weldline results from the meeting of two melt fronts flowing into each other from opposite directions, and a film-gated rectangular plaque mold with a circular insert that divides the melt front in two. Following the recombination of the fronts, there is additional flow as the melt fills the mold cavity. Two preparations containing 75 vol % of polyamide-6 and 25 vol % of polyethylene with and without compatibilizer were studied. In the first case, a compatibilizer was incorporated into the polyethylene prior to compounding with the polyamide-6. In the directly molded tensile bar the minor phase is strongly oriented parallel to flow. Only in the core, which represents about 10% of the sample thickness, do the dispersed phase particles assume spherical shape. The morphology of the weldline is closely related to that of the skin: the elongated structures are oriented parallel to the weldline plane. The effect of the compatibilizer on the mechanical properties (without the weldline) of the directly molded tensile bars is minor: it is overshadowed by the flow-induced morphology. The weldline strength loss is about 40% in the noncompatibilized blend. The introduction of the compatibilizer has restored the material's ability to yield and the properties are close to those measured without the weldline. For the second type mold, the effect of the weldline is less pronounced and the effect of the distance from the insert is negligible. The anisotropy is quite pronounced in the noncompatibilized blend. In compatibilized blends, all tensile properties are unaffected by the presence of weldline, except for the 2-mm-thick plaque in the position close to the insert. The properties in the direction parallel to flow are similar to the type I mold and not affected by the increase of plaque thickness. Consequently one may question the utility of the directly molded tensile specimens in studying various aspects of the mechanical behavior of multiphase materials where the flow-generated structure is very different from that found in "real" injection molded parts. © 1995 John Wiley & Sons, Inc.

INTRODUCTION

There is a strong relationship between the morphology and properties of immiscible polymer blends. The size and shape of the minor phase affects many properties; namely, the impact strength, ductility, and barrier properties, as well as flow behavior. The morphology of the dispersed phase can be influenced to varying degrees by interfacial modification, viscosity and elasticity ratios, composition, and the processing history.[1-3]

* To whom correspondence should be addressed.

Journal of Applied Polymer Science, Vol. 57, 1319–1332 (1995)
© 1995 John Wiley & Sons, Inc. CCC 0021-8995/95/111319-14

During processing of these materials, both phases can be deformed and oriented. When processed by the injection molding process, the flow of the molten polymer inside a cold mold generates a complex morphology throughout the thickness:[4]

- two outside "skin" layers formed by the expansion and rapid solidification of the melt front;
- two subskin "shear" layers influenced by the high shear rate; and
- a central "core" layer which, undergoing less shearing during flow inside the mold and taking the longest time to solidify, has a structure closest to that obtained under quiescent solidification.

Injection-molded parts may also contain defects known as weldlines or knitlines. They result from the union of two separated flow fronts. Weldlines in injection-molded polymer blends are not well documented. In his review paper on the application of polymer blends, Robeson[5] reported that in complex molds, the elimination of weldlines is virtually impossible, and very poor retention of strength (specially impact strength) is observed. Weldlines have been referred to as being the "Achilles' heel" of immiscible polymer blends. Loss of strength and toughness due to the presence of weldlines may be a problem in some homogeneous materials as well, but in multiphase materials such as polymer blends, filled and reinforced polymers, or liquid crystal polymers, the strength loss is usually much more pronounced. The weldline region is known to be structurally different from the rest of the material.[6,7]

When immiscible blends are evaluated by measure of the ductility, the impact strength always shows a negative departure from additivity rule.[8] Addition of an appropriate compatibilizer helps to recover the lost strength and ductility and is often accompanied by some loss of the yield strength and of the stiffness.[9-12] In order to evaluate the performance of such systems, samples must be prepared for mechanical testing. Different approaches are available:

- direct injection molding of samples required by the standard method (e.g., tensile samples defined by ASTM D638 standard method); and/or
- machining samples from molded plaques or from molded parts.

Undoubtedly because of the convenience, the mechanical properties of plastics are most often studied using directly molded dogbone-shaped tensile specimens. The flow-induced structure has a profound effect on the mechanical behavior of these samples. For instance, as was reported earlier,[13] during tensile and tensile impact loading, failure is initiated in the shear zone along the skin–core boundary. Because of the flow difference between the directly molded samples and the ones machined from plaques, one might expect differences in their behavior. For instance, Fisa et al.[14] reported a similar comparative study on noncompatibilized polypropylene/polycarbonate blends. The hypothesis of flow-induced orientation can be used to explain the differences observed between the properties of the samples machined from plaques and those directly molded into the tensile samples. The machined samples exhibit lower stiffness and strength. In the end-gated tensile sample cavity the melt convergence, as it enters the narrower section, must impart additional orientation and elongation to the dispersed phase. Fracture occurs in the area where the melt exits from the narrow section, where the diverging flow starts to orient the elongated structures in the direction perpendicular to flow.[14]

The subject of injection-molded polymer blends containing weldlines is not as well documented as its counterpart in virgin homopolymers. Injection-molded EPDM/PP systems with weldlines obtained from double-gated molds were studied by Thamm,[15] who reported an absence of the minor phase (EPDM) in the weldline region. Similar results were reported later by Malguarnera and Riggs.[16] They attributed the absence of the dispersed EPDM in the weldline region to a deficiency in the flow-front region, although this was never supported experimentally. Paul et al.[8-10] have studied the effect of a compatibilizer on the mechanical properties of several systems with and without weldlines obtained in a double-gated molds. Karger-Kocis and Csikai[13] studied the structure–properties relationships and the phenomena causing rupture of injection molded blends of EPDM/PP with and without weldlines. The usual skin–core structure was found. Two zones were observed in the skin: a thin PP layer on the surface, and a subskin with highly elongated rubber particles. The core was rich in rubber particles. This effect was attributed to the existence of a concentration gradient due to crystallization of the front in contact with the mold surface. During crystallization the polypropylene rejected the rubber particles instead of engulfing them. Similar morphological observations were carried out in this laboratory in a preliminary study on HDPE polyamide-6 (PA6) compatibilized with an

ionomer,[17] although a crystallization mechanism was not considered.

In this work we study the mechanical behavior of injection-molded HDPE/PA6 blends with and without weldlines as well as the influence of a compatibilizer. The detailed study of the morphology of these materials is being published separately.[18] The principal conclusions are:

- At a microscopic level, the morphology of the weldline zone differs significantly from the rest of the material. For example: in 4-mm-thick plaques, three distinct layers are observed away from the weldline. A skin originating from the expansion of the melt front is about 100 μm thick in the compatibilized blend and 300 μm in the noncompatibilized blend.
- The minor phase in the skin region is so finely divided as to be invisible even from scanning microscopy. However, the measurements by differential scanning calorimetry (DSC), by X-ray photoelectron spectroscopy (XPS), and by solvent extraction reveal that the concentration is relatively constant throughout the molded part.[18-20] In the subskin, the morphology is much coarser due to shear-induced coalescence. In the core, a spherical morphology predominates.
- The morphology gradient observed throughout the thickness, i.e., fine dispersion in the skin, coarse in the subskin (shear), and intermediate in the core, is also found as one moves away from the weldline to the bulk of the molded part. The width of the weldline zone is roughly twice that of the skin, suggesting again that in these blends the weldline is formed by the meeting of two laterally expanding melt fronts. Consequently, the weldline region shows a very similar morphology to that observed in the skin.

In spite of the immense technological importance of polymer blends, little work has been published on both compatibilized and noncompatibilized blends during injection molding, and particularly in the presence of weldlines. The objective of the present paper is to consider the mechanical characteristics—including those of weldlines—of two injection-molded polymer blends and their relationship to morphology. Directly molded tensile samples and those machined from rectangular plaques are used. The parameters to be investigated are the thickness of the plaque and the flow-path length.

EXPERIMENTAL

Materials

PA6 (Zytel 211; Dupont Canada, Inc.) with a number average molecular weight of M_n = 25000 was used. A high-density polyethylene from Dow Chemical Canada (Dow 06153C) having a melt flow index of 6.3 g/10 min, M_n = 20200, and M_w = 81300 was selected as a minor phase. The compatibilizing agent was an ionomer (Surlyn 9020; Dupont Canada, Inc.) terpolymer consisting of 80% polyethylene and 20% methacrylic acid–isobutyl acrylate mixture. The methacrylic acid was 70% zinc-neutralized. The polyethylene was stabilized with 0.2% antioxidant (Irganox 1010; Ciba Geigy). Glass beads (untreated and silane treated), obtained from Potters, were used as fillers in complementary experiments. The average bead diameter is about 45 μm.

Compounding

An initial dispersion of antioxidant in polyethylene was made by mixing their dry blend in a single-screw extruder. Then, using a twin-screw extruder, 10 vol % of the ionomer (I) was admixed to the stabilized and granulated PE. Finally, 25 vol % polyethylene (PE) with or without compatibilizer, or 25 vol % of glass beads, were incorporated into PA6. Prior to a typical mixing operation, the sample mixture was dried overnight at 90°C under vacuum to minimize hydrolytic degradation of the polyamide during processing. The polymer blending was carried out on a ZSK-30 (Werner-Pfleiderer) intermeshing, co-rotating twin-screw extruder with a screw length to diameter ratio, L/D of 40. Feeding was performed under nitrogen and vacuum was applied in the decompression zone. The blending conditions can be found in Fellahi et al.[18,20] Neat PA6 was twin-screw extruded to give it the same thermal history as the PA6 in the blends.

Injection Molding

The injection molding machine used was a Battenfeld type BA-C 750/300, with a clamping force of 80 tons. Two experimental molds, both with interchangeable cavities, were employed. A rectangular plaque (127 mm × 76 mm × 2, 4, and 6 mm cavity depth) was used. It is provided with a 2-mm-deep flash gate fed via a trapezoidal duct with a section varying from 30 to 50 mm^2. Tensile test bars were cut at different locations and termed as Type II specimens (Fig. 1). To produce plaques with weldlines a 6-, 12-, or 18-mm-diameter circular insert

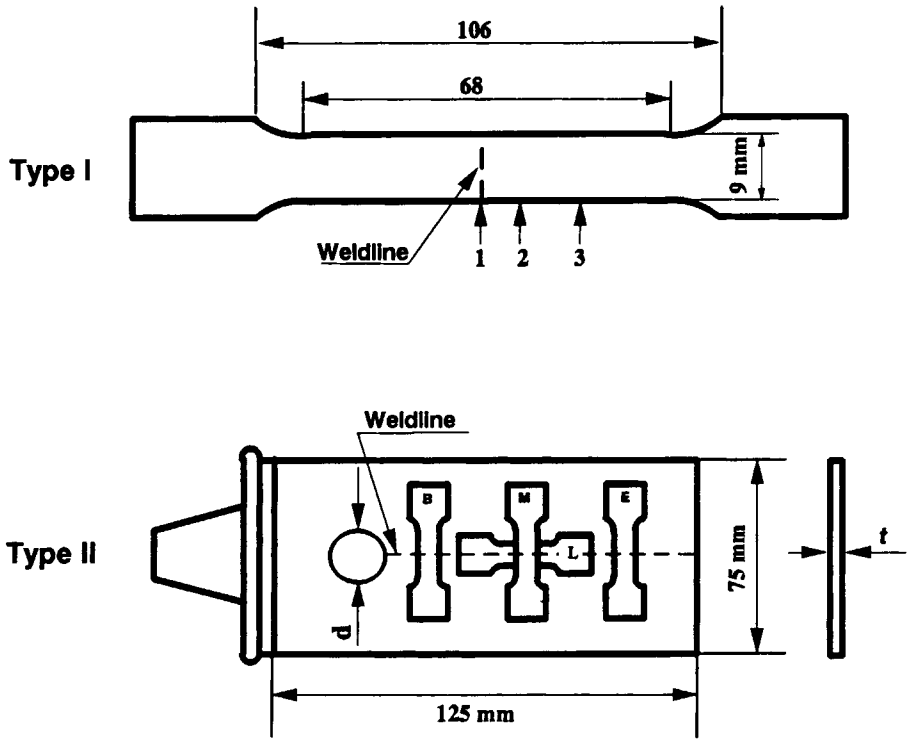

Figure 1 Mold cavities used in this work. Type I: Directly molded tensile specimens. Type II: Rectangular plaque with locations at which samples were machined. Plaque thickness: (t): 2, 4, and 6 mm; insert diameter (d): 6, 12, and 18 mm.

was installed in the cavity. Directly molded 3-mm dogbone tensile bars (Type I in Fig. 1) were molded using one or two gates to make samples with or without weldlines. As-received neat PA6, HDPE, and the prepared compounds were injection molded. The molding conditions are the same for both types and are reported elsewhere.[19,20]

Tensile Testing

Prior to testing all samples were conditioned at 23°C and 50% relative humidity for several days. The ASTM D638 standard was followed. Type I samples were tested directly while a special dogbone-shaped sample was designed to make the best use of the Type II plaques. Samples were machined transversally at different positions (B, M, and E) and longitudinally (L) from plaques with and without weldlines, as illustrated in Figure 1. A universal tensile machine was used with a crosshead speed of 5 mm/min and a 2.5 kN maximum load, to generate both ultimate tensile properties, with the secant modulus at 0.2%. For the latter case, an MTS extensometer (632.13C.20) with a 10-mm gauge length was used. The load and axial and lateral extension were recorded by data acquisition software. The strains recorded using extensometers are referred to as *axial* and *lateral* strains. The term *apparent* strain refers to the strain calculated using the crosshead displacement and the gauge length of the sample. Unless indicated, the stress–strain axial and the volume strain–axial strain tests were stopped before fracture (at $\epsilon_a = 10\%$).

To study local stiffness variations along the sample, the extensometer was placed either on or outside the weldline at positions 1, 2, and 3, as indicated by the numbered arrows in Figure 1. Directly molded dogbone specimens were used in this test.

Tensile Dilatometry

The tensile test was carried out according to ASTM D638 M. The volume-change measurement was carried out during the tensile test using the above-mentioned axial extensometer, and an Instron transverse extensometer, model 2640.007. It is assumed that the deformation in the thickness is equal to that in the width.[21] Both extensometers were attached to the specimen. Lateral and axial extension were recorded simultaneously on a PC using data acquisition software. From the axial strain (ϵ_a), and the transverse strain (ϵ_t) one can compute the volume strain ($\Delta V/V_0$) as:

$$\Delta V/V_0 = (1 + \epsilon_a)(1 + \epsilon_t)^2 - 1 \quad (1)$$

Scanning Electron Microscopy

Samples with and without compatibilizer were studied and were prepared as follows:

- Freeze-fracture: a small rectangular strip from each sample was placed in liquid nitrogen for 10–15 min, and then fractured manually.
- Microtoming and solvent extraction: rectangular samples (1 × 1.5 × 0.5 cm) were cut with a Reichert Jung Supercut 2050 microtome equipped with a glass knife. First, each sample was frozen in liquid nitrogen for 15 min. During the cutting operation, the temperature was kept at approximately −100°C to reduce the extent of surface deformation. The microtomed samples were immersed for 1 h in decalin at 120°C to dissolve the polyethylene (minor phase). Following the extraction the samples were dried in a vacuum oven for 24 h to remove the solvent.
- Fracture surfaces of samples broken in a tensile test.

Sample surfaces, after being coated with a layer of Gold/Palladium, were examined under a Jeol 8645 type scanning electron microscope at 10 Kv.

RESULTS AND DISCUSSION

Double Gated (Type I Mold)

In neat polyamide and in the compatibilized blend, the weldline was invisible to the naked eye except for a V-notch of a variable depth. The depth of the V-notch is related to the distance from the vents located in the middle of the cavity (along the weldline area). The side of the sample which coincides with the mold parting line does not have a V-notch, while at the opposite side, the V-notch is almost 100 μm deep. This observation confirms the role that trapped air, compressed by the expanding melt fronts, plays in the formation of the V-notch.[22–24] In the noncompatibilized blend the weldline region is more opaque than the rest of the sample. It was observed that the higher opacity of the weldline area, which is predominantly located in the core of the weldline, develops during the later part of the cooling cycle. The presence of this more-opaque zone indicates that the residual stresses, resulting from the nonisothermal solidification during the cooling stage, are sufficient to induce debonding of the matrix–minor phase interface.[25] The higher opacity is evidently related to the presence of microvoids in the weldline zone.

The morphology of the noncompatibilized blend is shown in Figure 2. Away from the weldline [Fig. 2(A)], the minor phase particles are elongated and oriented parallel to flow in the skin and subskin regions. The orientation is particularly pronounced in the skin where the polyethylene particles are stretched into sheetlike formations. In the core, which represents only about 10% of the sample thickness, spherical shape predominates. The section of the weldline area is shown in Figure 2(B). It is obvious that the morphology of the weldline is closely related to that of the skin. The weldline, having been formed by the collision of two opposing melt streams, also shows the minor phase keeping the shape and orientation it acquired during the melt front expansion. In Figure 2(B) a 50-μm-thick layer, where the minor phase is more finely divided, sep-

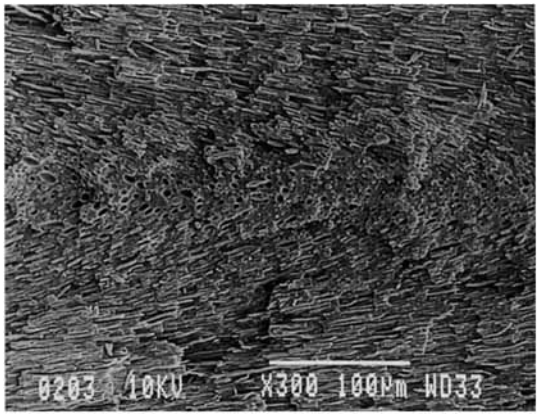

Figure 2 Micrographs of type I noncompatibilized blend (NC)-perpendicular to flow view. (A) no weldline; (B) with weldline.

arates the two melt fronts. The morphology of the compatibilized blend is quite similar to that of its noncompatibilized counterpart. The main difference between the blends is the size of the minor phase formations—the compatibilized blend exhibits a much finer morphology.[1,2]

The results of the tensile tests on these directly molded samples are summarized in Table I. The stress vs. apparent strain curves are shown in Figure 3. To draw the curves in Figure 3 (as well as those shown in Figs. 12, 13, and 14 for Type II specimens), the strain was simply assumed to be proportional to the crosshead displacement. The neat PA6 is not affected by the presence of the weldline. Its behavior is similar to that reported for other semicrystalline, ductile plastics such as polyamide-66, polypropylene, high-density polyethylene, etc.[26,27] In this study it was found that the mechanical properties of PA6 are somewhat affected by the passage through the twin-screw extruder. For this reason the property values given for neat PA6 are those of the extruded polymer. It is believed that partial devolatilization of the plasticizer may be the cause of the slightly higher stiffness of the twin-screw extruded and injection-molded samples (compared to those made by molding of as-received pellets).

The effect of the compatibilizer appears negligible in samples without weldlines: both materials follow the same path (curves C and NC, Fig. 3) until well beyond the yield point; the only difference being a higher elongation at break of the compatibilized sample (250% vs. 100% for the noncompatibilized blend). In both blends, the post-yield deformation occurs via homogeneous yielding of the entire gauge length, as is the case of neat nylon-6. The effect of the compatibilizer is much more visible in samples with weldlines (curves C–WL and NC–WL, Fig. 3). Although at small strains both materials also follow

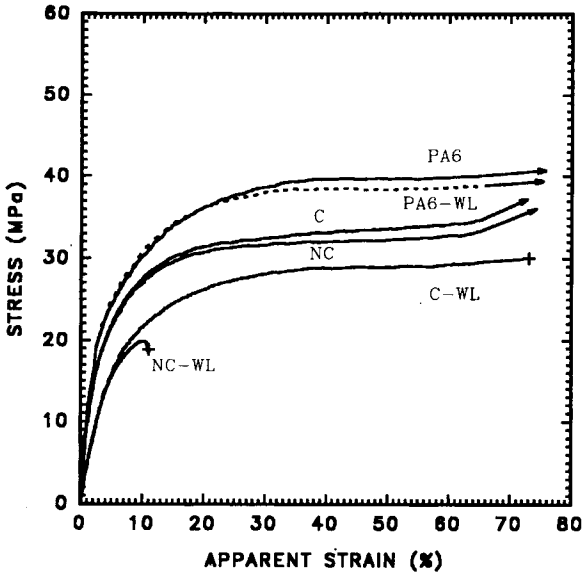

Figure 3 Stress/strain curves of type I samples with (WL) and without weldline PA6, compatibilized (C) and noncompatibilized (NC) blends.

the same path, the noncompatibilized sample breaks at the weldline before the onset of yield. The addition of the compatibilizer has restored the ability of the material to yield in the presence of a weldline, but the sample still ends up breaking in the weldline at an overall strain of 80%. Considering the structure of the weldline area as shown in Figure 2(B), one would expect the fracture to develop along the elongated structures oriented parallel to the weldline. This does not seem to be the case. The overall view of the fracture surface is shown in Figure 4. In the outer zone, which represents about 75% of the cross-sectional area, the matrix exhibits significant microstretching [Fig. 5(A)]. In the inner zone, the fracture occurred in a brittle manner [Fig. 5(B)].

Table I Tensile Properties for Type I Samples

Material	E (GPa)	σ_y (MPa)	ε_y (%)	σ_b (MPa)	ε_b (%)
PA6	0.90/1.4*	39	45	62	220
PA6-WL	0.90	39	35	59	200
NC	1.20	32	40	40	100
NC-WL	1.10	no yield	no yield	24	10
C	1.20	33	40	58	270
C-WL	.90	29	45	32	80
PA6NTGB	1.70	19	2.2	NA	NA
PA6TGB	2.0	25	NA	NA	NA

NC = without compatibilizer; C = with compatibilizer; WL = with weldline.

Standard deviations: modulus, E—3%; yield stress, σ_y—3%; stress-at-break, σ_b—5%; apparent strain at yield, ε_y—15%; apparent strain at break, ε_b—25% of reported values.

NA: not available.

*: PA6 twin screw extruded.

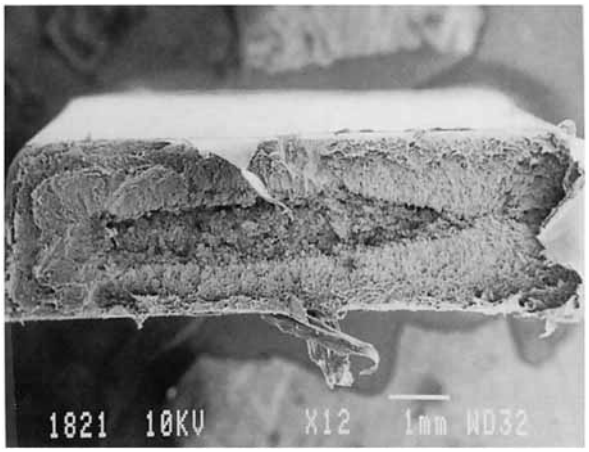

Figure 4 Micrograph of noncompatibilized (NC) blends, type I specimens. Fracture surface at the weldline. General view perpendicular to flow.

Most of the PE particles in this zone are loose and do not show any evidence of plastic deformation. As mentioned above, the PE particles in the core, which is under tensile stress generated during cooling, probably separated from the matrix before the test had even begun. Occasionally an amoeboid PE formation can be found, [Fig. 5(C)] but these are clearly in a minority. Thamm reported similar structures oriented perpendicular to flow.[15] Fracture surfaces of compatibilized samples are analogous to those of their noncompatibilized counterparts. In the outside layer the PE particles have deformed along with the matrix [Fig. 6(A)], while the core reveals the presence of well-adhered but undeformed polyethylene particles [Fig. 6(B)]. As with the noncompatibilized blend, the fracture surface of the core shows little evidence of ductility. It appears that the fracture starts in the sample interior where the material is under triaxial stress, rather than at the V-notch, and consequently it cannot yield as already reported in the literature.[13] Following the fracture of the core, the material near the surface is able to stretch, as evidenced by the appearance of fracture surfaces.

Comparison of various materials used in this work at small strains provides valuable insights into their behavior. The stress-vs.-axial-strain curves are shown in Figures 7, 8, 9, and 10. To draw these curves, the strain was assumed to be identical to the extensometer displacement. Figure 7 shows the stress–strain curves of both blends, of the PA6 filled with 25 vol % of glass beads (untreated and silane treated), as well those of both starting materials (PE and PA6). In the polyamide containing poorly adhering glass beads (curve GB–NT), the stress reaches a maximum at about 2% strain. The yield stress of this material is approximately equal to that of the unfilled polyamide reduced by the factor representing the area occupied by glass beads.[28] It was shown that at yield, essentially all the glass beads debonded from the matrix.[28] When glass beads are treated with silanes little or no debonding takes place in the range of strains considered,[28] and the stress borne by the material at a given strain exceeds that of the neat PA6 (curve GB–T). The curves of both blends show appearances similar to that of the treated, glass-bead-filled PA6. Both curves (C and

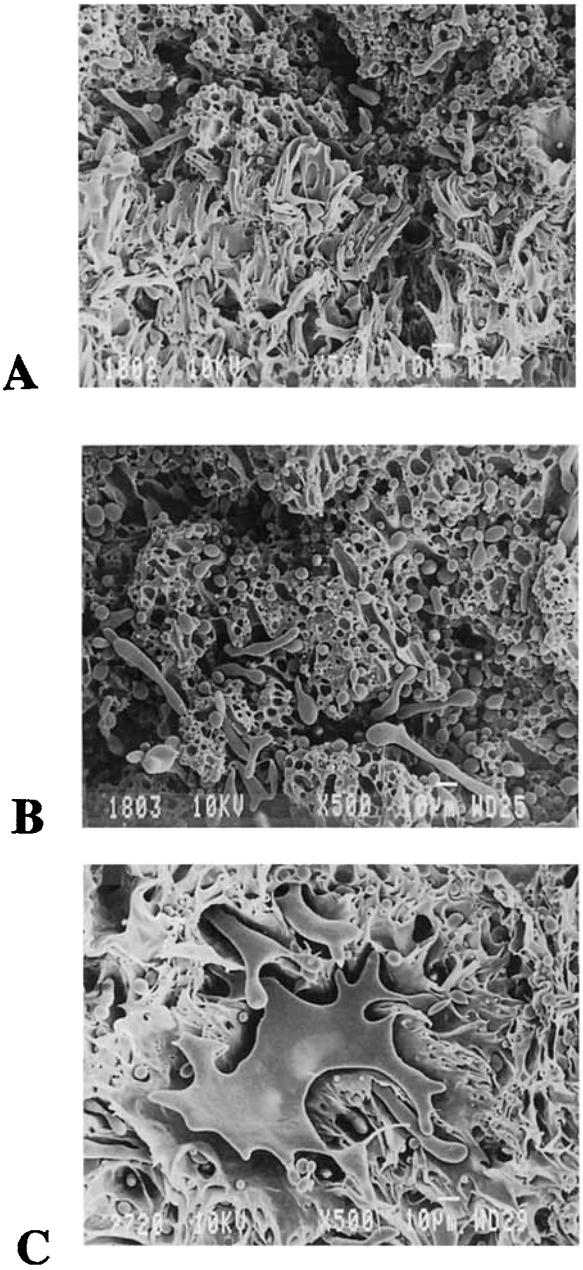

Figure 5 Micrographs of fractured surfaces of tested type I noncompatibilized (NC) specimens containing a weldline (perpendicular to flow view). (A) skin; (B) and (C) core.

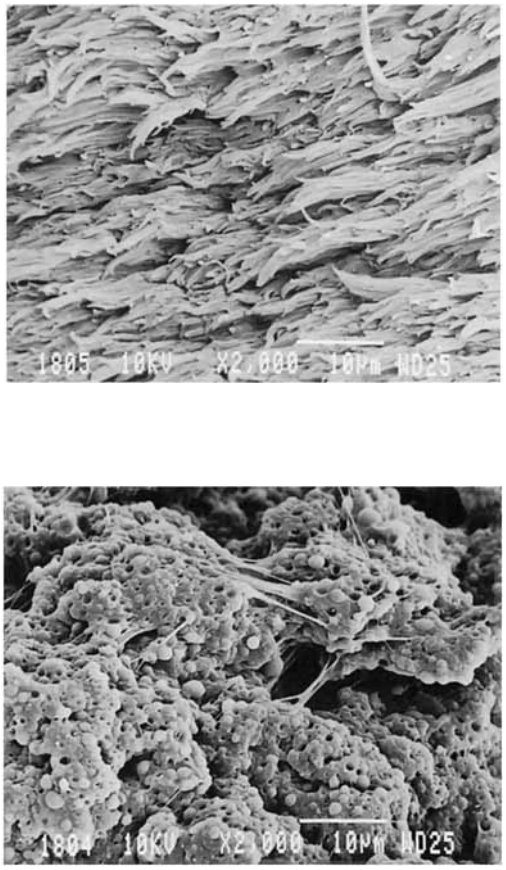

Figure 6 Micrographs of fractured surfaces of compatibilized (C) blends, type I specimens, containing a weld-line (perpendicular to flow view). (A) skin; (B) core.

NC) follow very closely that calculated using the rule of mixtures:

$$\sigma_b = \sigma_{PA}\Phi_{PA} + \sigma_{PE}\Phi_{PE} \quad (2)$$

This curve is identified as Eq. 2 in Figure 7 where σ_b, σ_{PA}, and σ_{PE} are stresses measured at a given strain in the blends, neat PA6, and neat HDPE, respectively; while Φ_{PA} and Φ_{PE} are their volume fractions (0.75 and 0.25, respectively).

This result shows that in both blends tested under these conditions the dispersed phase bears its share of stress. This may seem surprising in light of the data obtained by the tensile dilatometry (Fig. 8). The volume strain recorded with the compatibilized blend is small. In fact, it is similar to that recorded for both the neat polymer and the polymer filled with treated glass beads. With untreated glass beads and with the noncompatibilized blend (NC), the interfacial debonding begins at about the same level of strain, i.e., 1.5%. However, the material filled with untreated beads dilates at a faster rate than the noncompatibilized blend. Despite the debonding, the

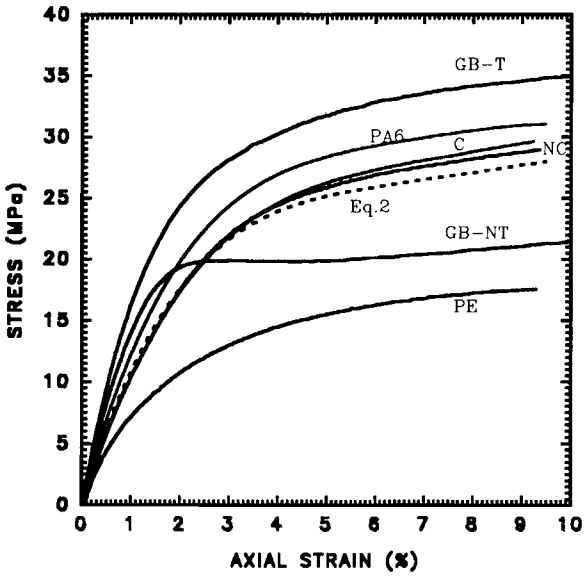

Figure 7 Stress vs. axial strain curves of type I samples. Neat HDPE (PE), PA6, compatibilized (C), noncompatibilized (NC), filled PA6 with treated (GB-T) and untreated (GB-NT) glass beads, and (- - -) equation 2.

dispersed phase of the noncompatibilized blend can bear the same load as its compatibilized counterpart. This observation suggests that with this sample shape the mechanical behavior is dominated by the flow-induced morphology. An elongated particle of variable cross-section and shape (see also Fig. 5) trapped in the matrix has no choice but to deform along with the matrix, in spite of the lack of interfacial adhesion. Consequently, one can question the

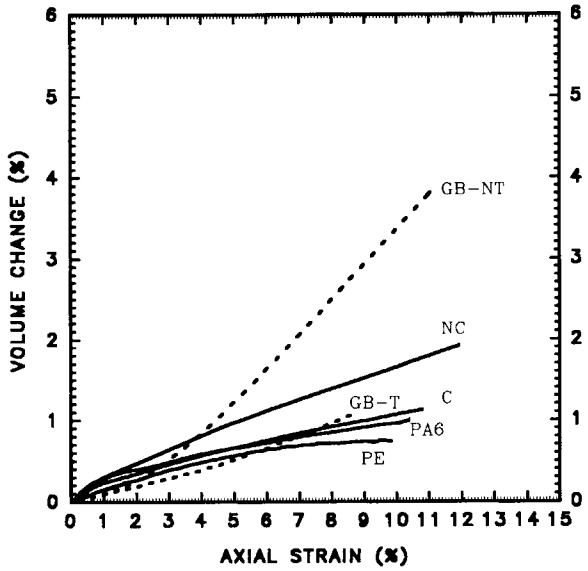

Figure 8 Volume change versus axial strain of type I specimens. (Notation same as in Fig. 7.)

utility of the directly molded tensile specimens to study various aspects of the mechanical behavior of multiphase materials where the flow-generated structure is very different from that which is found in "real" injection-molded parts.

Conventional methods used to evaluate the weldline strength consist of dividing the weldline sample's yield stress (breaking stress in the absence of yield) by that of a sample without the weldline.[34] This approach indicates a strength loss of 40% for the noncompatibilized sample and 10% for the compatibilized sample. Monitoring tensile properties by placing extensometers on and away from the weldline and by studying how the strain develops during the constant strain rate test sheds a slightly different light on the situation. With the noncompatibilized blend (Fig. 9), the stress–strain curve of the weldline area overlaps that measured away from the weldline up to a stress of about 15 MPa. Above 15 MPa the weldline area starts to deform at a faster rate and the sample breaks at 24 MPa, when the strain away from the weldline is only about 7%. Similar behavior has been observed for glass-filled PA6.[26]

Figure 10 shows the results obtained with the compatibilized blend. In this case the curves are identical. It can be said, therefore, that the behavior of the weldline area in the compatibilized blend is identical to that of the material away from the weldline, and consequently the weldline effect is negligible.

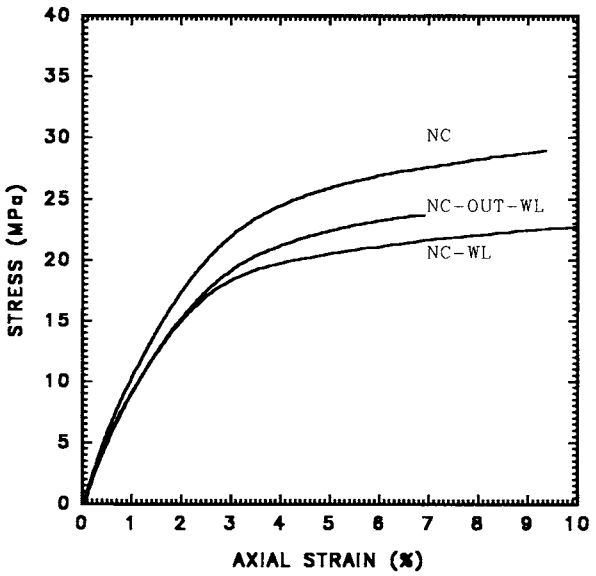

Figure 9 Effect of the weldline and the extensometer location on the stress–strain curve for type I specimens of noncompatibilized blends: without weldline, position 1 (NC); with weldline, position 1 (NC–WL); with but outside the weldline, positions 2 and 3 (NC–OUT–WL). This last sample broke at an axial strain of 7%.

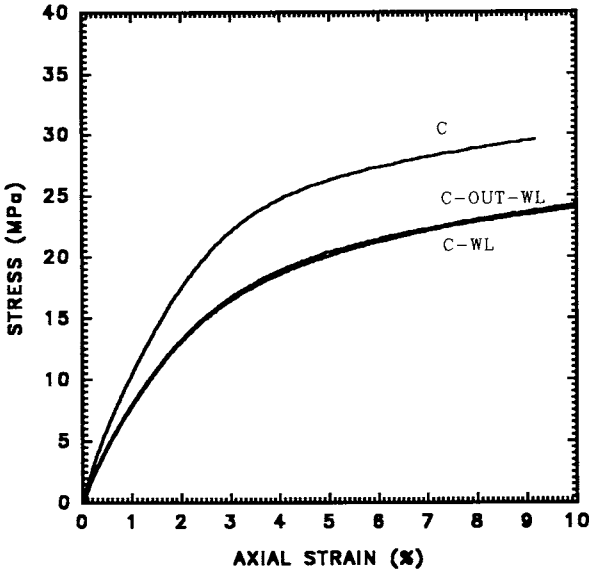

Figure 10 Effect of the weldline and the location of the extensometer on the stress–strain curves of type I specimens of compatibilized (C) blends. (Notation same as in Fig. 9.)

It is now necessary to consider the differences between the samples molded with the weldline (two-gate cavity) and without the weldline (one gate). Figures 3, 9, and 10, and Table I show that the initial stiffness is lower when the cavity has two gates not only in the weldline, but also away from the weldline. Since the injection rate is identical for all these samples (0.42 cm^3/s), the melt velocity in the cavity when one gate is used is twice that of the two-gate cavity. Complementary experiments in which the injection rate was doubled (with the two-gate cavity) were performed to determine the effect of melt velocity on the stress–strain curves. The results show that this effect is negligible. Other workers have also reported that melt velocity in the cavity does not affect the tensile properties (stiffness and stress).[11] It appears, therefore, that the morphology and the mechanical properties of both blends are affected by the overall thermomechanical history of the measured area. With one gate the melt flows through the entire cavity length and the melt front penetrates the wider cavity area opposite the gate. Intuitively, one would expect the orientation to be higher than in the case of the two-gate mold, where the tested area comprises two immobilized melt fronts in the weldline and material that travelled a shorter distance and was at a higher temperature at the end of the mold-filling stage.

Finally, it is worth noting that the elastic moduli for samples without weldlines are not affected by

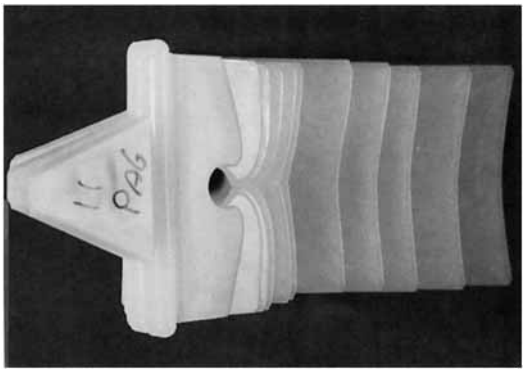

A

B

Figure 11 Short-shots of type II mold with 4 mm thickness and 12 mm insert diameter, obtained with: (A) neat PA6; and (B) compatibilized blends (HDPE/Ionomer/PA6).

addition of the compatibilizer. Similar results have been reported for other multiphase systems.[29,30]

Plaques (Type II)

Although the weldlines are nearly invisible to the naked eye in plaques molded using cavities with an insert, and although one would like to believe that the molten polymer forgets the insert at a certain distance behind it, this is not the case with the blends used in this work. Differences in the mold-filling patterns can be evidenced by short-shot experiments. Figure 11 shows the short shots obtained with the matrix and with the compatibilized blend. With PA6 [Fig. 11(A)] and with HDPE, the junction of the two melt fronts vanishes at a short distance behind the insert and the melt front recovers a straight profile. With both blends, the junction persists during the entire mold-filling stage [Fig. 11(B)]. This unexpected mold-filling behavior has been also reported with fiber-and-platelet-filled PP[31] and glass-fiber-reinforced PA66.[26] It indicates that, as with other multiphase systems, the melt in the weldline zone advances at a slower pace than in other areas of the plaque, suggesting that the local viscosity of the melt behind the insert is higher than elsewhere, offering more resistance to flow. One of the consequences of the higher viscosity and the slower melt advancement is that the weldline plays a role similar to that of the wall and that the weldline is formed by adjacent melt fronts depositing onto each other. Yokoi et al.[32] have studied the evolution of the angle between the melt front with the distance from the insert. They stated that when the "weldline vanishing angle value" is reached, the weldline has effectively disappeared.

The mechanical behavior of noncompatibilized and compatibilized blends (2-, 4-, and 6-mm-thick samples) cut transversally to flow with (for 4 mm only) and without weldline is shown in Figures 12 and 13, respectively. Results for samples cut longitudinally to flow are gathered in Figure 14. Tensile properties are presented in Table II. The results can be summarized as follows:

- The effect of the weldline on the properties is much less pronounced than indicated by the directly molded samples (type I).
- In noncompatibilized blends (Table II), the yield stress is reduced by only about 15% in position B, immediately behind the insert, when

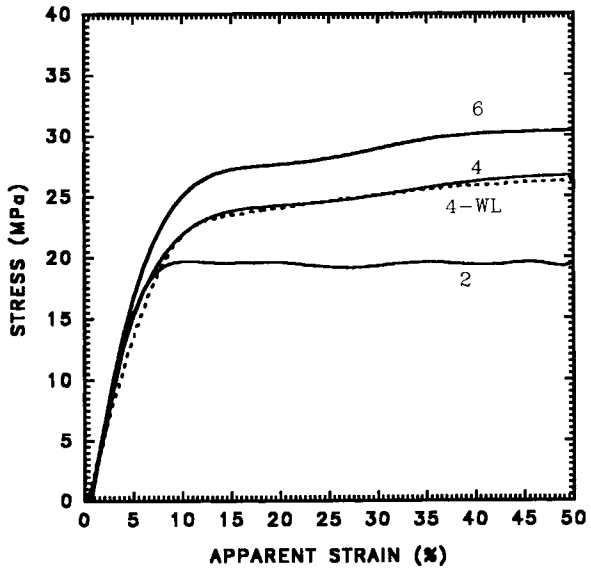

Figure 12 Stress–strain curves for noncompatibilized blends (NC), type II specimens. Plaque thickness: 2, 4, and 6 mm; insert diameter: 12 mm. Transverse direction (M). Weldline in the 4-mm-thick shaped: 4–WL.

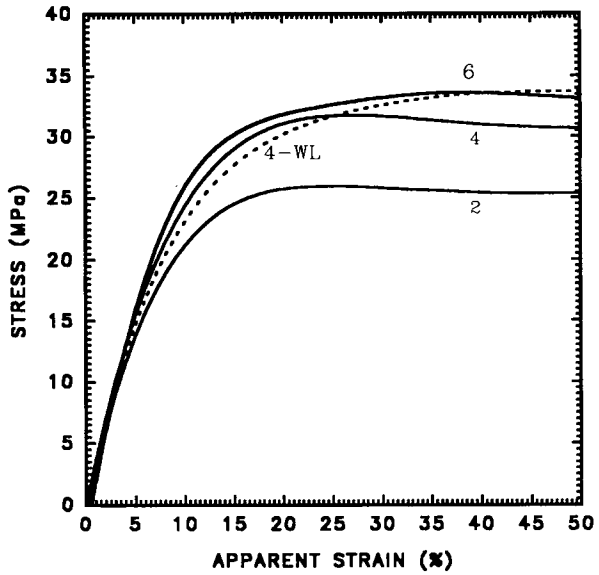

Figure 13 Stress–strain curves for compatibilized blends, type II specimens. Plaque thickness: 2, 4, 6 mm; insert diameter: 12 mm. Weldline in the 4-mm-thick plaque: 4–WL.

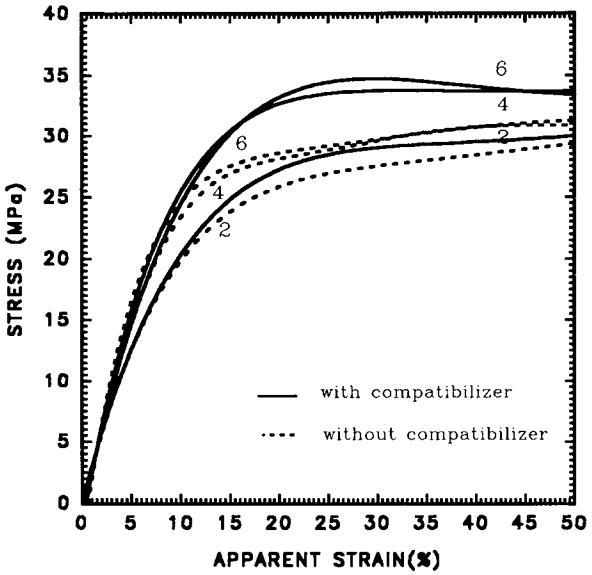

Figure 14 Stress–strain curves for noncompatibilized (NC) and compatibilized (C) blends, type II specimens. Plaque thickness: 2, 4, and 6 mm. In the longitudinal direction: —— with compatibilizer; - - - without compatibilizer.

compared to a sample without a weldline. This difference becomes even smaller for positions farther away from the insert (Fig. 12).

- Noncompatibilized blends show significant strength anisotropy—the yield stress recorded in the direction parallel to flow (position L, Table II) is about the same as that recorded in type I samples (i.e., $\approx$ 30–33 MPa). In addition, the yield stress parallel to flow is independent of the plaque thickness except in the 2 mm case. The yield stress perpendicular to flow (e.g., position M) is only about 20 MPa for the 2-mm plaques. It is about 25 MPa when the thickness is 4 mm. At 6 mm thickness, the yield stress anisotropy disappears. The effect of the thickness on the yield stress is more pronounced in this direction (i.e., transverse to flow) as shown

Table II Tensile Properties of Type II Samples (Insert Diameter d = 12 mm) as a Function of Positions B, M, E, and L (see Fig. 1)

Position	t (mm)	σ_y (MPa)		ε_y (%)		σ_b (MPa)		ε_b (%)	
		NC	C	NC	C	NC	C	NC	C
B	2	18/21	26/26	14/18	55/34	19/20	26/34	15/100	60/230
	4	21/26	34/30	14/75	40/35	27/23	33/33	25/150	140/140
	6	26/29	34/32	20/27	55/34	30/30	34/35	55/65	100/130
M	2	20/20	26/26	20/11	31/22	17/21	31/34	47/56	180/230
	4	23/23	31/31	13/21	42/22	26/28	34/35	75/140	180/140
	6	25/27	34/33	46/20	31/32	31/32	38/34	85/85	140/110
E	2	19/21	26/25	19/21	33/30	19/21	38/38	38/59	210/260
	4	25/26	33/30	49/85	25/28	25/31	36/40	50/160	130/210
	6	28/28	33/32	32/30	33/30	29/33	37/38	60/110	170/180
L	2	29/28	29/29	31/42	21/34	47/45	48/>50	140/220	190/>250
	4	28/28	34/34	27/37	18/26	48/45	50/54	140/120	140/260
	6	30/28	34/34	51/40	21/26	46/38	51/47	100/130	150/240

t = sample thickness; NC = without compatibilizer; C = with compatibilizer.

The first and second values in each column are for samples with and without weldlines, respectively. Average standard deviations are similar to those reported in Table I.

in Figures 12 and 14. Menges et al.[33] have attributed this phenomenon to the competition between flow-induced orientation and crystallinity. In the thinner plaque, the effect of orientation on the yield stress predominates, while in thicker plaques a crystallization effect prevails.

The initial slopes of the stress–strain curves are relatively independent of both the plaque thickness and of the direction (Figs. 12, 13, and 14). The curves start to deviate at the onset of yield. This suggests that yielding coincides with the beginning of the debonding process.

- In compatibilized blends the weldline effect essentially disappears; all tensile properties are unaffected by the presence of the weldline. The only exceptions to this are the 2-mm-thick plaques in the position close to the insert where the weldline sample breaks without appreciable yielding. The weldline free sample, however, undergoes significant homogeneous yielding. The yield stress is independent of the plaque thickness and orientation except for the 2-mm-thick plaque (Figs. 13 and 14).
- The effect of insert diameter on the yield strength has been found to be negligible in both blends.

The effect of the compatibilizer on interfacial adhesion is shown in Figure 15. These pictures were obtained by fracturing the samples at liquid nitrogen temperature. In the noncompatibilized blend [Fig. 15(A)] the fracture surface exhibits loosely held, completely debonded PE particles. With the compatibilized blend [Figs. 15(B) and 15(C)], the fracture path went through the dispersed phase. It is very interesting to note that the surface of the broken polyethylene particles in the compatibilized blend contains small ($\approx$ 0.2 μm) spherical formations. The most likely explanation for this observation is that some of the compatibilizer contained in the polyethylene exuded as the material was brought to room temperature.

Micrographs of fracture surfaces on the tested samples of both blends are shown in Figures 16 and 17. In the noncompatibilized blends, the bulk of the minor phase appears undeformed through the entire thickness. Despite the fact that the material deformed by 70%, the fiberlike formations in the outer layers and the spherical ones in the core are well separated from the matrix. Only occasionally in the outer layer do the fibers show evidence of cold drawing (see arrows, Fig. 16[B]). This observation and

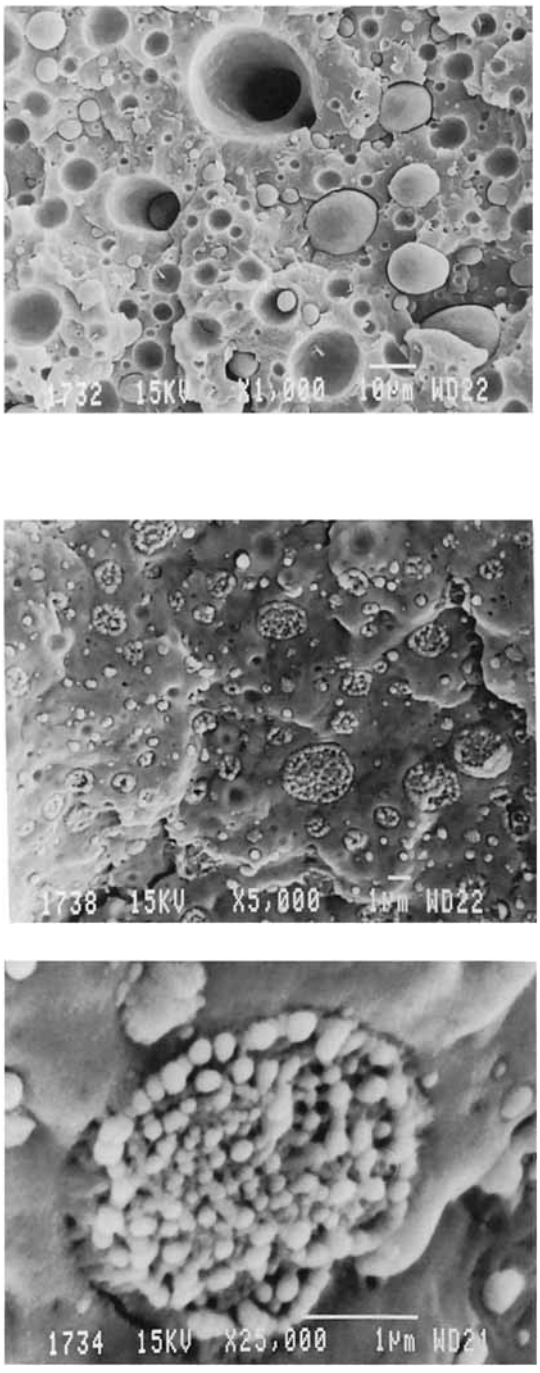

Figure 15 Micrographs of freeze-fractured, untested, 4-mm-thick samples. (A) noncompatibilized (NC), parallel to flow view; (B) compatibilized (C) blend, perpendicular to flow view; and (C) magnification (× 25,000).

the fact that the yield stress is generally lower than that predicted by the rule of mixtures show that the debonding occurred well before the onset of yield. The transition between the core, where the polyethylene is spherical, and the outer layers, where elongated predominate, is clearly visible.

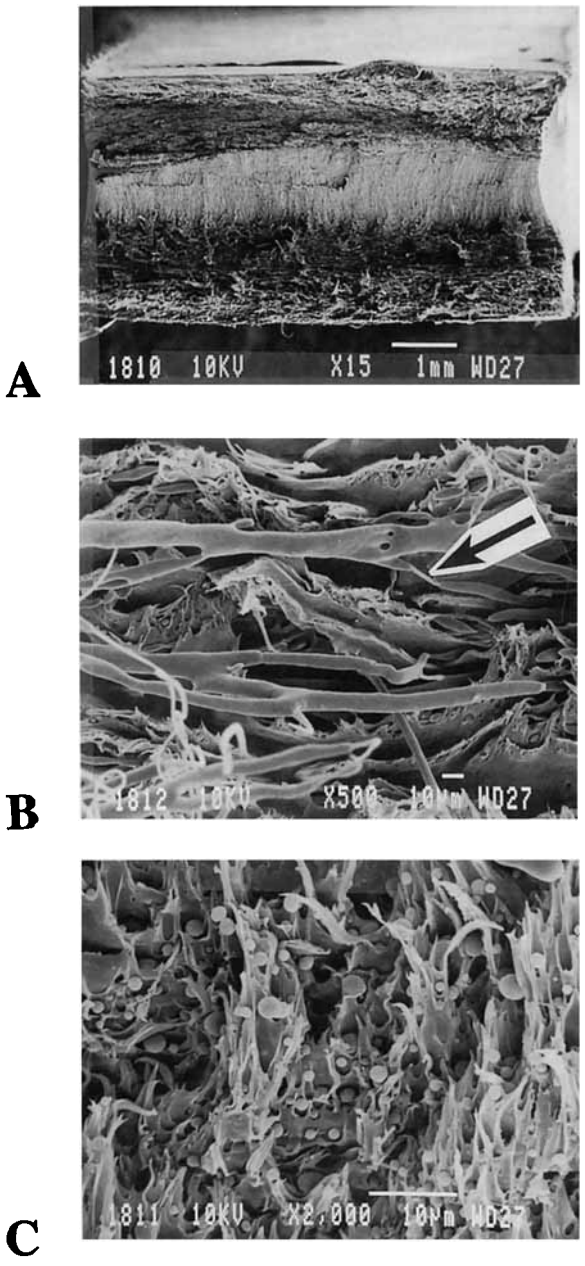

Figure 16 Micrographs of fracture surfaces of tested noncompatibilized type II specimens containing a weldline (position M). (A) whole cross-section; (B) skin; (C) core.

With the compatibilized blends (Fig. 17), the fracture surfaces do not show evidence of microstretching. A highly oriented subskin is shown in Figure 17(B). In the core, the dispersed phase is spherical and much finer [Fig. 17(C)]. The yield stress is about the same as the one observed in type I samples. This confirms that in the compatibilized blend the dispersed phase adhesion to the matrix is sufficient to prevent significant debonding until at least the yield point.

CONCLUSION

The measured effect of the compatibilizer on the mechanical properties of injection-molded high-density polyethylene/polyamide-6 depends greatly on the mold shape and on testing direction. In directly molded tensile samples without weldlines, the highly stretched polyethylene particles oriented parallel to the applied stress bear their fraction of stress, and the yield stress is independent of the

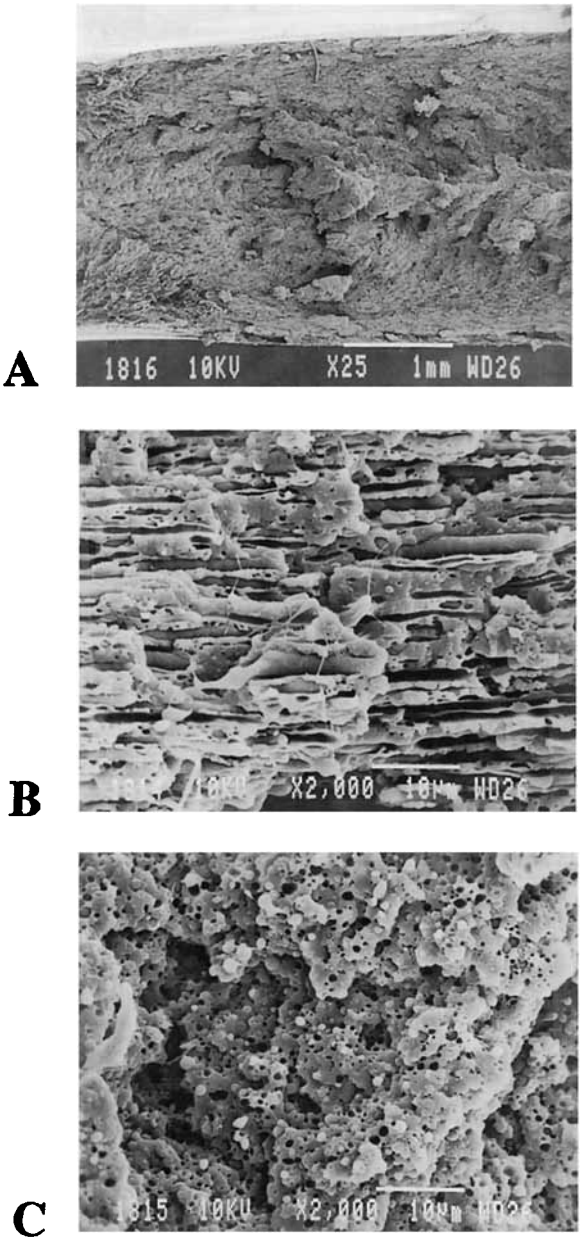

Figure 17 Micrographs of fracture surfaces of tested compatibilized blends, type II specimens, containing a weldline at position M. (A) whole cross-section; (B) skin; and (C) core.

presence of the compatibilizer. The strength loss due to the presence of the weldline is about 40% in the absence of compatibilizer in directly molded tensile samples but becomes negligible when compatibilizer is added.

When test specimens are machined from molded plaques in which the weldline was produced by placing a circular insert to divide the flow, the weldline effect is much less pronounced. In the absence of the compatibilizer, a strength loss of about 15% is recorded (compared to samples machined from the plaque without an insert). In addition, the uncompatibilized blend exhibits significant flow anisotropy. The compatibilized blend is essentially isotropic and maintains the same strength in the presence of the weldline.

REFERENCES

1. L. A. Utracki, *Polymer Alloys and Blends: Thermodynamics and Rheology,* Hanser Publishers, Munich, 1989, Chap. 1.
2. B. D. Favis, *Can. J. Chem. Eng.,* **69,** 619 (1991).
3. P. Van Gheluwe, B. D. Favis, and J.-P. Chalifoux, *J. Mat. Sci.,* **23,** 3910 (1988).
4. Z. Tadmor, *J. Appl. Polym. Sci.,* **18,** 1753 (1974).
5. C. Robeson, *Polym. Eng. Sci.,* **27,** 1591 (1987).
6. B. Fisa, in *Composites Materials and Technology, Processing and Properties,* P. K. Mallick and S. Newman, Eds., Hanser Publishers, Munich, 1990, Chap. 9, p. 265–320.
7. R. Boukhili and R. Gauvin, *Plast. Rubber Process. and Appl.,* **11,** 17 (1989).
8. E. Nolley, J. W. Barlow, and D. R. Paul, *Polym. Eng. Sci.,* **20,** 364 (1980).
9. D. W. Bartelett, J. W. Barlow, and D. R. Paul, *J. Appl. Polym. Sci.,* **27,** 2351 (1982).
10. C. R. Lindsay, D. R. Paul, and J. W. Barlow, *J. Appl. Polym. Sci.,* **26,** 1 (1981).
11. B. Brahimi, A. Ait-Kadi, and A. Ajji, *SPE ANTEC Tech. Papers,* **37,** 1129 (1991).
12. R. Armat and A. Moet, *Polymer,* **34,** 977 (1993).
13. J. Karger-Kocsis and I. Csikai, *Polym. Eng. Sci.,* **27,** 241 (1987).
14. B. Fisa, B. D. Favis, and S. Bourgeois, *Polym. Eng. Sci.,* **30,** 1051 (1990).
15. R. C. Thamm, *Rubb. Chem. Tech.,* **50,** 24 (1977).
16. S. C. Maguarnera and D. C. Riggs, *Polym. Plast. Tech. Eng.,* **17,** 193 (1981).
17. B. Fisa, A. Bouti, B. Favis, and F. Lalande, *SPE ANTEC Tech. Papers,* **37,** 1135 (1991).
18. S. Fellahi, B. D. Favis, and B. Fisa, *Polymer,* to appear.
19. S. Fellahi, Ph.D. Thesis, École Polytechnique de Montréal, 1994.
20. S. Fellahi, B. Fisa, and B. D. Favis, *SPE ANTEC Tech. Papers,* **39,** 211 (1993).
21. S. Y. Hobbs, M. E. J. Dekkers, and V. H. Watkinson, *J. Mat. Sci.,* **23,** 1225 (1988).
22. G. D. Gilmore and R. S. Spencer, *Modern Plastics,* **4,** 117 (1951).
23. L. R. Schmidth, *Polym. Eng. Sci.,* **14,** 797 (1974).
24. E. D. Hagerman, *Plast. Eng.,* **10,** 67 (1973).
25. P. G. Charalambides, *J. Am. Ceram. Soc.,* **73,** 1674 (1990).
26. A. Meddad and B. Fisa, *Polym. Eng. Sci.,* to appear.
27. J. P. Trotignon, J. L. Lebrun, and J. Verdu, *Plast. Rubb. Proc. Appl.,* **2,** 1249 (1982).
28. A. Meddad, S. Fellahi, M. Pinard, and B. Fisa, *SPE ANTEC Tech. Papers,* **40,** (1994).
29. P. Vollenberg, D. Hienkens, and H. C. B. Ladan, *Polym. Comp.,* **9,** 382 (1988).
30. E. A. A. Van Hartingsvelt, Ph.D. Thesis, Delft University, The Netherlands, 1987.
31. B. Fisa and M. Rahmani, *Polym. Eng. Sci.,* **31,** 1330 (1991).
32. H. Yokoi, H. Watanabe, and K. Oka, *SPE ANTEC Tech. Papers,* **37,** 367 (1991).
33. G. Menges, A. Troost, J. Koske, H. Ries, and H. Stabrey, *Kunstst. Ger. Plast.,* **78,** 806 (1988).
34. R. M. Criens and H. C. Mosle, *Polym. Eng. Sci.,* **23,** 591 (1983).

Received April 18, 1994
Accepted March 8, 1995